pubs.acs.org/Biomac

Article

Coordinative Double Hydrophilic All-Polyether Micelles for pH-Responsive Delivery of Cisplatin

Jiwoo Yoon and Byeong-Su Kim*

Cite This: https://doi.org/10.1021/acs.biomac.3c01301

Read Online

ACCESS | Metrics & More | Article Recommendations | Supporting Information

ABSTRACT: Despite its widespread use in the treatment of numerous cancers, the use of cisplatin still raises concerns about its high toxicity and limited selectivity. Consequently, the necessity arises for the development of an effective drug delivery system. Here, we present an effective approach that introduces a double hydrophilic block copolyether for the controlled delivery of cisplatin. Specifically, poly(ethylene glycol)-*block*-poly(glycidoxy acetic acid) (*m*PEG-*b*-PGA) was synthesized via anionic ring-opening polymerization using the oxazoline-based epoxide monomer 4,4-dimethyl-2-oxazoline glycidyl ether, followed by subsequent acidic deprotection. The coordinative metal−ligand interaction between cisplatin and the carboxylate group within the PGA block facilitated the formation of micelles from the double hydrophilic *m*PEG-*b*-PGA copolyether. Cisplatin-loaded polymeric micelles had a high loading capacity, controlled pH-responsive release kinetics, and high cell viability. Furthermore, in vitro biological assays revealed cellular apoptosis induced by the cisplatin-loaded micelles. This study thus successfully demonstrates the potential use of double hydrophilic block copolyethers as a versatile platform for biomedical applications.

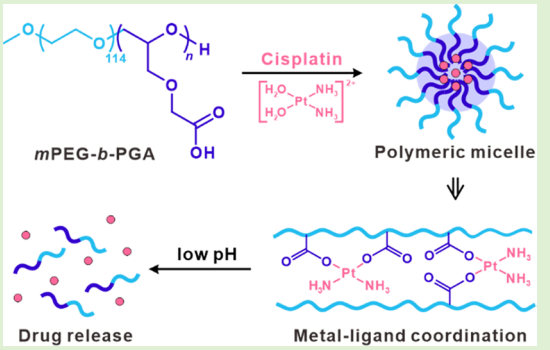

INTRODUCTION

Cisplatin is one of the most widely used chemotherapeutic drugs for the treatment of malignant tumors in the breast, liver, testicle, ovary, and other organs.[1,2] It activates cellular apoptosis by forming inter- and intrastrand cross-links with DNA.[1,3,4] However, the use of cisplatin can lead to nephrotoxicity and neurotoxicity while also promoting drug resistance among cancer cells.[3,5] Therefore, it is necessary to develop innovative strategies to reduce the toxicity of cisplatin while enhancing its therapeutic efficacy.

Nanoparticles have emerged as a promising vehicle for drug delivery because they can improve the efficacy of a drug, reduce its side effects, and prevent drug resistance. Nanoparticles can also penetrate further into a tumor with a low lymphatic clearance due to their enhanced permeability and retention (EPR) effect, resulting in passive targeting.[6] Nanoparticles that are composed of inorganic materials, such as gold and quantum dot nanoparticles, possess unique physical and optical properties that are beneficial in sensing with their own therapeutic effect.[7] Polymeric micelles, on the other hand, have garnered particular attention for their ease of preparation and modification, along with a wide range of polymer types available.[8] Polymeric micelles are often composed of amphiphilic polymers, wherein hydrophobic domains self-assemble to form the micellar core that enables the encapsulation of hydrophobic drugs, while the hydrophilic segments constitute the outer shell.

Alternatively, the recent development of double hydrophilic block copolymers (DHBCs) has opened up new possibilities for drug delivery systems.[9] DHBCs consist of two distinct hydrophilic blocks, a system that can lead to high water solubility and enhanced biocompatibility, permeability, and excretion.[10] While one of these blocks typically enhances the solubility of the DHBC, the other block is responsive to the surrounding conditions (e.g., the ionic strength, pH, and temperature).[11] In particular, DHBCs with ionic blocks readily self-aggregate into nanoscale micelles[12−14] and exhibit improved stability under physiological conditions due to their ability to maintain their micellar form through cross-linking with metal ions, even below the critical micelle concentration.[15] For example, poly(ethylene oxide)-*b*-poly(acrylic acid) (PEO-*b*-PAA) and poly(ethylene oxide)-*b*-poly(methacrylic acid) (PEO-*b*-PMA) are well-known anionic DHBCs capable of self-assembly via ionic interactions that are responsive to external pH conditions.[16,17] The DHBC of PEO-*b*-PAA has been complexed with Gd^{3+} ions as an MRI contrasting agent and as a drug carrier for doxorubicin and

Received: November 27, 2023
Revised: January 29, 2024
Accepted: January 30, 2024

Scheme 1. Schematic Representation of the Design and Preparation of pH-Responsive Double Hydrophilic Polymeric Micelles for Coordination with Cisplatin and Its Controlled Release with Concomitant Disassembly

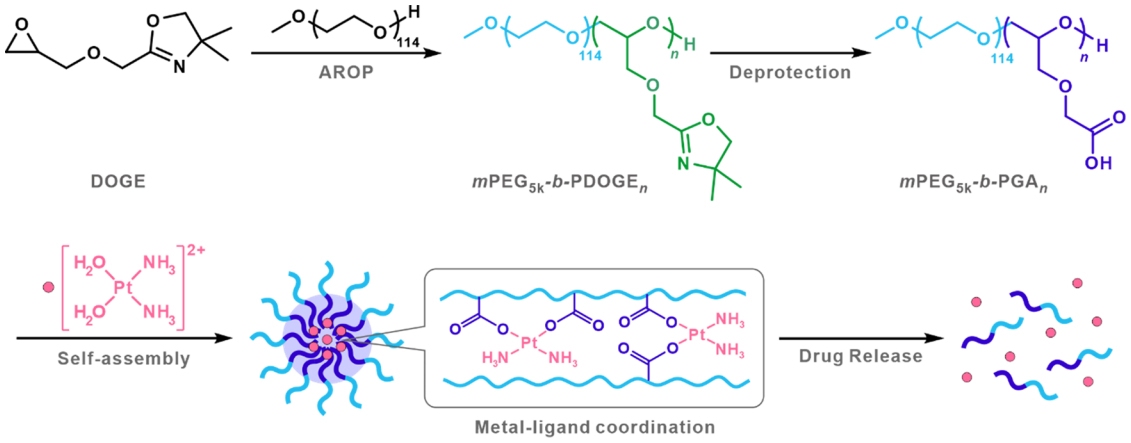

mitoxantrone.[18,19] PEO-*b*-PMA ionomer complexes have also been developed as core-cross-linked polymeric micelles with Ca^{2+} to improve their stability.[20]

A pioneering work in the use of polymeric micelles for cisplatin delivery was demonstrated by Kataoka and co-workers, who developed poly(ethylene glycol) (PEG) and poly(glutamic acid) (PGA) copolymers capable of encapsulating cisplatin.[21] Subsequently, numerous studies have reported the development of cisplatin-loaded carriers using PEG-*b*-PGA block copolymers.[22,23] Meanwhile, Stenzel and colleagues employed poly[oligo(ethylene glycol) methyl ether methacrylate]-based polymers with carboxylate functionalities to conjugate with cisplatin.[24,25] In addition, a pH-responsive polymeric micelle system containing poly(ethylene oxide)-*b*-poly(α-carboxylate-ε-caprolactone) was developed for the slow release of cisplatin, reducing its cytotoxicity.[26]

Polyether-based copolymers have also emerged as novel cisplatin carriers based on the numerous advantages of PEG for biomedical applications, including high biocompatibility, the prevention of aggregation, and longer circulation times.[27] Chau et al. designed PEG-*b*-polyglycidol copolymers modified with malonate groups to chelate cisplatin and thus reduce the associated toxicity, hemolysis, and side effects.[28] However, postpolymerization modification to carboxylates was not achieved in a controlled manner, and the process involved multiple steps. Moreover, a carboxyl-modified hyperbranched polyether, namely poly[3-methyl-3-(hydroxymethyl)oxetane], has been reported, which suffers from low aqueous solubility due to the presence of hydrophobic groups.[29] While these micelles exhibit a higher therapeutic efficacy than free cisplatin in terms of reduced toxicity and a pH-responsive release profile, there remains a need to produce polymeric micelles that consist of all-hydrophilic polymers by a simple method.

Herein, we report all-polyether-based diblock copolymer micelles for use in a cisplatin delivery system. By taking advantage of 4,4-dimethyl-2-oxazoline glycidyl ether (DOGE), a novel functional epoxide monomer with oxazoline as a protecting group,[30] we prepared a series of poly(ethylene glycol)-*block*-poly(glycidoxy acetic acid) (*m*PEG-*b*-PGA) DHBCs after deprotection. The self-assembly of the polymeric micelles was primarily driven by the coordinative interaction of cisplatin and carboxylate moieties within the polymers. Most importantly, cisplatin was released at a low pH, leading to the selective targeting of cancer cells due to the acidic conditions near tumors (Scheme 1). Combined with its low toxicity and enhanced solubility, this DHBC approach leads to the controlled induction of apoptosis pathways, contributing to the suppression of cancer cells.

EXPERIMENTAL SECTION

Materials and Reagents. Tetrabutylammonium hydrogen sulfate ($TBAHSO_4$), 2-amine-2-methyl-1-propanol, calcium hydride (CaH_2), poly(ethylene glycol) methyl ether (*m*PEG; M_n: 5000 g/mol), phosphazene base *t*-BuP_4 solution, *cis*-diamminedichloroplatinum(II) (cisplatin), silver nitrate, phosphate-buffered saline (PBS, pH 7.4), *o*-phenylenediamine (OPD), 4′,6-diamidine-2′-phenylindole dihydrochloride (DAPI), and paraformaldehyde were purchased from Sigma-Aldrich and used as received unless otherwise noted. Glycolic acid and epichlorohydrin were obtained from Tokyo Chemical Industry, and hydrochloric acid (35%, w/w) was purchased from Daejung. Amberlite IR-120(H) was purchased from Alfa Aesar, and PBS (pH 7.4, 1×) for in vitro assays and propidium iodide (PI) were purchased from Thermo Fisher Scientific. Toluene collected from a solvent purification system (Vacuum Atmospheres) was dried over molecular sieves (3 Å) before use. *m*PEG was purified with AmberLite MAC-3 H Cation Exchange Resin from Sigma-Aldrich prior to use. Deuterated $CDCl_3$ and D_2O NMR solvents were purchased from Cambridge Isotope Laboratories.

Characterizations. ^{1}H NMR (400 MHz) and ^{13}C NMR (101 MHz) spectra were recorded on a Bruker NMR spectrometer at room temperature. All spectra were acquired by using $CDCl_3$ (δH = 7.26 ppm and δC = 77.16 ppm) and D_2O (δH = 4.79 ppm) as internal standards. Gel permeation chromatography (GPC) measurements were taken using an Agilent 1200 series with tetrahydrofuran (THF) as the eluent at 30 °C at a flow rate of 1.0 mL/min with a refractive index (RI) detector. FT-IR spectra were recorded on an Agilent Cary 630 equipped with an attenuated total reflection (ATR) module. Dynamic light scattering (DLS) measurements were performed using a Zetasizer Nano analyzer (Malvern) with a solid-state laser (λ = 633 nm) at an angle of 90 °C. The size and morphology of the micelles were examined using atomic force microscopy (AFM; NX10, Park Systems) in noncontact mode. Inductively coupled plasma-mass spectrometry (ICP-MS) was used to determine the quantity of platinum at trace levels using an Agilent 7900 series instrument. UV−vis spectra were recorded to quantify the released cisplatin in a PBS solution using a UV−vis spectrometer (RF-6000, Shimadzu). MTT assays were conducted using a multilabel plate reader (Victor 5, PerkinElmer) at an absorbance of 570 nm. Apoptosis assays were conducted using

https://doi.org/10.1021/acs.biomac.3c01301
Biomacromolecules XXXX, XXX, XXX−XXX

Table 1. Characterization of the *m*PEG-*b*-PDOGE Copolymers and Deprotected *m*PEG-*b*-PGA Copolymers Synthesized in This Study

polymer code	composition	$M_{n,NMR}$[a,b] (g/mol)	$M_{n,GPC}$[c] (g/mol)	$Đ$[c]	$M_{n,NMR}$[b,d] (g/mol)
P15*	$mPEG_{114}$-*b*-$PDOGE_{15}$	7800	6800	1.09	7100
P25*	$mPEG_{114}$-*b*-$PDOGE_{25}$	9600	8200	1.08	8000
P40*	$mPEG_{114}$-*b*-$PDOGE_{40}$	12,400	9600	1.08	10,500

[a]Determined via ^{1}H NMR spectroscopy in D_2O. [b]Determined by the ratio of the integral of the initiator protons to that of the methylene protons (x vs d' or d'' in Figure 2). [c]Determined from GPC measurements (THF, RI signal, and PS standard). [d]Deprotected polymer of *m*PEG-*b*-PGA measured using ^{1}H NMR spectroscopy in D_2O. Note that the deprotected polymers are referred to as P15, P25, and P40, respectively.

confocal light-scattering microscopy (CLSM; LSM 600, Carl Zeiss) and flow cytometry (BD FACS Aria Fusion, BD Life Sciences).

Synthesis of 4,4-Dimethyl-2-Oxazoline Glycidyl Ether (DOGE) Monomer. The synthesis of 4,4-dimethyl-2-oxazoline glycidyl ether was performed via two steps according to a method reported in a previous study.[30] In a 250 mL round-bottom flask equipped with a Dean−Stark apparatus, (4,4-dimethyl-4,5-dihydrooxazol-2-yl)methanol was synthesized by adding glycolic acid (5.97 g, 78.5 mmol) to a solution of 2-amine-2-methyl-1-propanol (7.49 mL, 78.5 mmol) in 125 mL of xylene. After the mixture was heated at 170 °C for 16 h, xylene was removed in vacuo, and the resulting viscous yellow mixture was purified by sublimation to yield the white solid (4,4-dimethyl-4,5-dihydrooxazol-2-yl)methanol (4.89 g, 37.86 mmol) with a yield of 48.2%. Following this, 13.63 g of NaOH was dissolved in 20.44 mL of water in a 500 mL round-bottom flask in an ice bath. $TBAHSO_4$ (0.63 g, 1.89 mmol) and epichlorohydrin (14.84 mL, 189.30 mmol) were added to a 40% aqueous NaOH solution and stirred for 30 min. (4,4-Dimethyl-4,5-dihydrooxazol-2-yl)methanol (4.89 g, 37.86 mmol) was then added slowly in an ice bath. The reaction was conducted at room temperature for 18 h. After extraction using ethyl acetate, the crude product was stored with CaH_2 overnight to remove the moisture, followed by distillation to yield a yellow oil consisting of the DOGE monomer (3.22 g, 17.36 mmol) in a yield of 45.87%. ^{1}H NMR (400 MHz, $CDCl_3$): δ 4.21 (m, 2H), 3.93 (s, 2H), 3.84 (dd, J = 11.6, 3.2 Hz, 1H), 3.43 (dd, J = 11.6, 6.0 Hz, 1H), 3.15 (m, 1H), 2.76 (dd, J = 4.8, 4.0 Hz, 1H), 2.57 (dd, J = 4.8, 2.4 Hz, 1H), 1.24 (s, 6H). ^{13}C NMR (101 MHz, $CDCl_3$): δ 162.92, 79.20, 72.00, 67.17, 65.61, 50.47, 44.09, 28.25.

Synthesis of the *m*PEG-*b*-PDOGE Block Copolymer. *m*PEG (M_n: 5000 g/mol) was used as a macroinitiator to synthesize the block copolymer. First, *m*PEG was purified to remove the shoulder peak from GPC analysis using AmberLite MAC-3 H Cation Exchange Resin in deionized water at 50 °C for 3 h, followed by filtration and freeze-drying. Purified *m*PEG (0.60 g, 0.12 mmol, 1.0 equiv) dried using azeotropic distillation was placed in a Schlenk flask under a flow of nitrogen. After this, 0.52 mL of dry toluene (2.5 M relative to DOGE) was added to the flask, and the mixture was stirred for 30 min at 60 °C. After cooling to 40 °C, a mixture of 0.09 mL of *t*-BuP_4 in *n*-hexane (0.8 M, 0.14 mmol, 1.2 equiv) was added to the solution and stirred for 15 min. DOGE (0.56 g, 3.0 mmol, 25 equiv) was then added dropwise to the solution. Polymerization was terminated by adding methanol after stirring for 12 h. The residual solvent was removed under vacuum, and the polymer dissolved in methanol was precipitated in cold diethyl ether, followed by concentration in vacuo (P15* in Table 1). ^{1}H NMR (400 MHz, D_2O): δ 4.18 (s, 50H), 4.07 (s, 50H), 3.70−3.58 (m, 581H), 3.33 (s, 2H), 1.24 (s, 150H).

Deprotection of *m*PEG-*b*-PDOGE. *m*PEG-*b*-PDOGE (100 mg, 0.0129 mmol, 1.0 equiv of oxazoline moiety) was reacted with 1.93 mL of 1.0 M HCl (5.0 equiv with respect to the oxazoline moiety) in methanol (1:1, v/v %) at room temperature for 24 h. The product was treated with Amberlite IR-120(H) to remove *t*-BuP_4 and deprotected products. Precipitation was then conducted in cold diethyl ether, with the polymer dissolved in methanol. The residues were removed via dialysis (Spectra/Por Dialysis Membrane Biotech CE Tubing (MWCO 500−1000 Da) with distilled water, producing *m*PEG-*b*-PGA (30 mg, 0.0043 mmol, P15 in Table 1) at a yield of 33.44%. ^{1}H NMR (400 MHz, D_2O): δ 4.22 (s, 50H), 3.73−3.66 (m, 581H), 3.34 (s, 2H).

Preparation of Polymeric Micelles. Cisplatin was pretreated to prepare aquated cisplatin *cis*-$[Pt(NH_3)_2(OH_2)_2]^{2+}$ using a previously reported procedure.[31] Initially, cisplatin was reacted with 2 equiv of $AgNO_3$ for 24 h at room temperature in the dark and centrifuged at 10,000 rpm for 1 h, followed by filtration through a 0.2 μm filter. Aquated cisplatin solution was then added to an aqueous solution of polymers (10 mg/mL, pH 7.0) with a 0.1−1.0 equivalence of cisplatin to the number of carboxylate units in the polymer ([COOH] = 3.0 mM in deionized water), followed by stirring at 37 °C for 24 h. Unbound cisplatin was removed using dialysis (Spectra/Por Dialysis Membrane Biotech RC Tubing, MWCO = 1000 Da) with deionized water for 2 days. The solution was filtered through a 0.20 μm filter and stored at 4 °C. The drug loading capacity was determined by using ICP-MS using the following equation:

$$\text{loading capacity (\%)} = \frac{\text{weight of cisplatin in micelles}}{\text{total weight of micelles}} \times 100\ (\%)$$

Cisplatin Release Analysis. Cisplatin-loaded polymeric micelles were dialyzed (Float-A-Lyzer dialysis device, MWCO = 3.5−5 kDa, 1.0 mL) with 200 mL of PBS (pH 7.4 and pH 5, respectively) at 37 °C under constant stirring. A 4 mL aliquot of the dialysate was withdrawn, and an equal amount of the same PBS was introduced to replace it at regular time intervals. The quantity of released cisplatin was determined using *o*-phenylenediamine (OPD) assays via absorption spectroscopy.[31] Specifically, 0.6 mL of the aliquot and 0.6 mL of the OPD solution (1.2 mg/mL) in *N*,*N*-dimethylformamide (DMF) were mixed and heated for 2 h at 100 °C in the dark. After the mixture was cooled to room temperature, the concentration of Pt complex was determined using UV−vis spectroscopy at 705 nm with a molar extinction coefficient of 79.21 mM^{-1} cm^{-1}.

Cytotoxicity Assays. L929 and A549 cells were grown in RPMI-1640 medium containing 10% FBS and 1% penicillin−streptomycin in a humidified incubator at 37 °C with 5% CO_2. The toxicity of the polymer and micelles was determined using 3,4,5-dimethylthiazol-2,5-diphenyltetrazolium bromide (MTT) assays. In a 96-well plate, L929 cells were seeded at 5 × 10^3 cells/well and incubated overnight. The polymer was added at different concentrations, and the cells were incubated for 24 h in the incubator. Subsequently, 100 μL of MTT solution with a final concentration of 0.5 mg/mL in PBS was added to the wells, and the cells were incubated for an additional 4 h. After the cell medium was carefully aspirated, 100 μL of DMSO was added to dissolve the formazan crystals from the living cells. The absorbance was measured by using a microplate reader at 570 nm. The cytotoxicity assays for micelles were conducted with an identical method using A549 cells for different incubation times.

Apoptosis Assays. A549 cells were seeded at a density of 5 × 10^4 cells/well on coverslips placed in 24-well plates. The required concentrations of free cisplatin and cisplatin-loaded micelles were then added to the cells. After incubation, the medium was removed, and the cells were washed three times with PBS. The cells were stained with 1.0 mg/mL of propidium iodide solution for 15 min in the incubator. The cells were then washed twice with PBS and fixed

https://doi.org/10.1021/acs.biomac.3c01301
Biomacromolecules XXXX, XXX, XXX−XXX

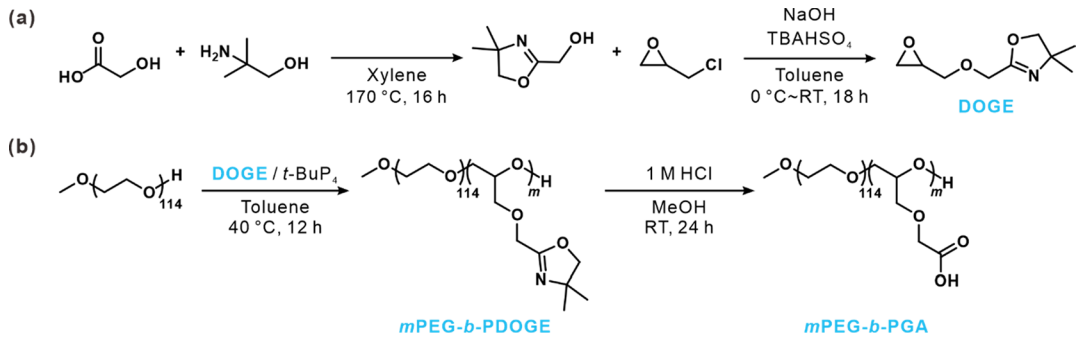

Figure 1. Synthetic scheme for the (a) DOGE monomer and (b) *m*PEG-*b*-PDOGE block copolymer and its subsequent deprotection under acidic conditions to yield *m*PEG-*b*-PGA.

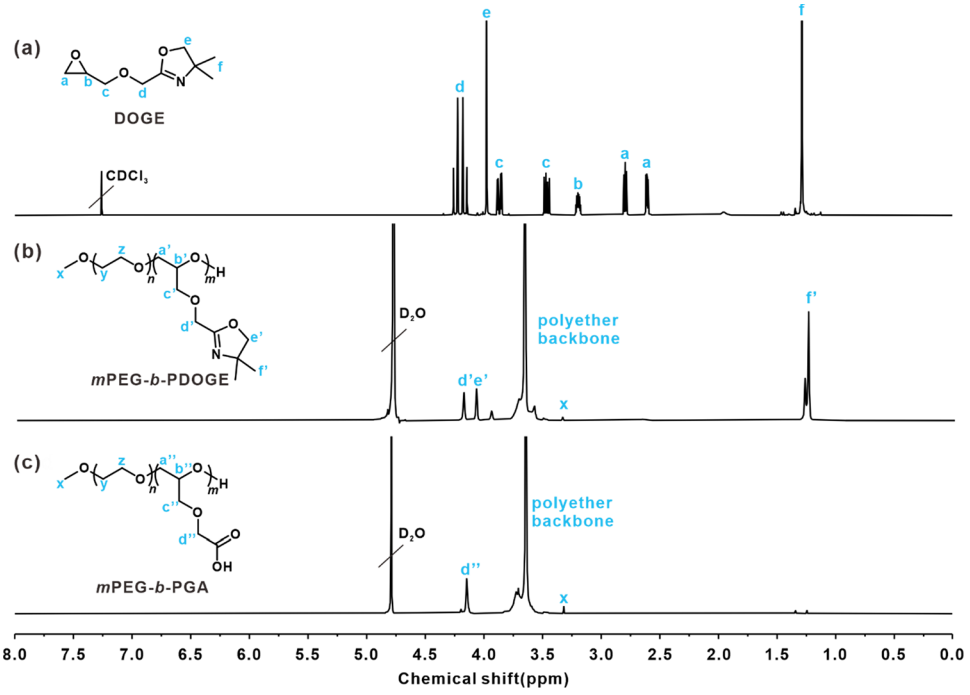

Figure 2. Representative ^{1}H NMR spectra of (a) DOGE monomer, (b) *m*PEG-*b*-PDOGE block copolymer (P25* in Table 1), and (c) deprotected *m*PEG-*b*-PGA block copolymer (P25 in Table 1). All spectra were collected in D_2O except for (a), which was measured in $CDCl_3$.

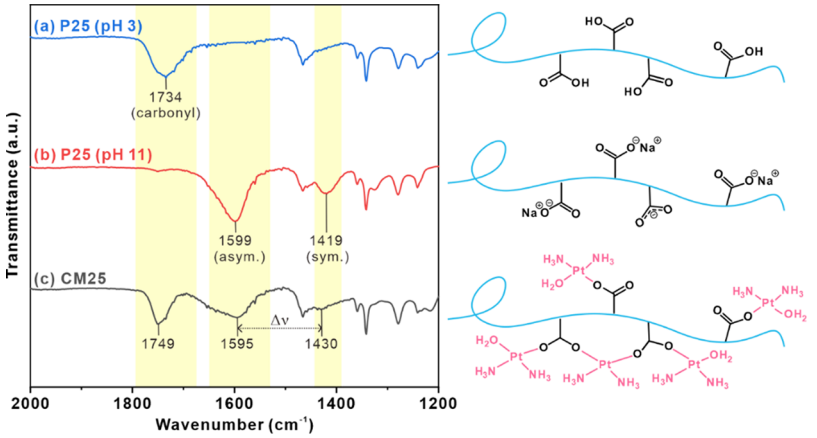

Figure 3. Representative FT-IR spectra for (a) P25 at pH 3, (b) P25 at pH 11, and (c) CM25, with the corresponding illustration of the coordination modes. Samples were prepared via lyophilization after purification.

with 4% paraformaldehyde for 10 min at room temperature. The cells were washed again with PBS twice and stained with 5 μg/mL DAPI solution for 5 min at room temperature in the dark. After washing with PBS three times, the coverslips were mounted using ProLong Glass Antifade Mountant (Invitrogen). The cells were carefully observed by using confocal microscopy.

https://doi.org/10.1021/acs.biomac.3c01301
Biomacromolecules XXXX, XXX, XXX−XXX

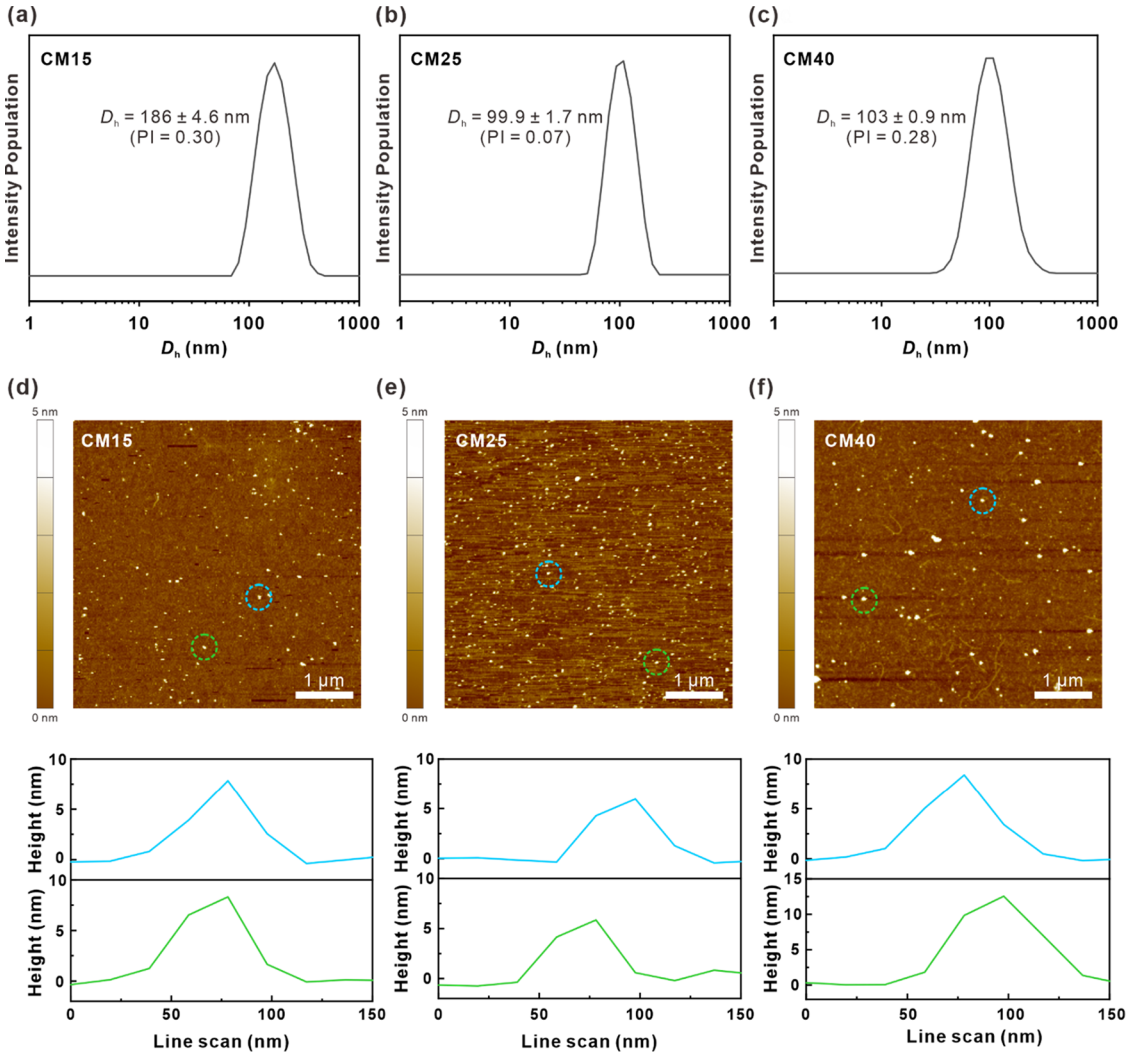

Figure 4. Size and morphology of cisplatin-complexed CM15, CM25, and CM40 micelles determined by using DLS and AFM. (a–c) Hydrodynamic diameter (D_h) of the (a) CM15, (b) CM25, and (c) CM40 micelles determined using DLS. Polydispersity index (PI) values are indicated. (d–f) Height-mode AFM images of the (d) CM15, (e) CM25, and (f) CM40 micelles, with the corresponding line scan profiles for the two micelles circled in each image.

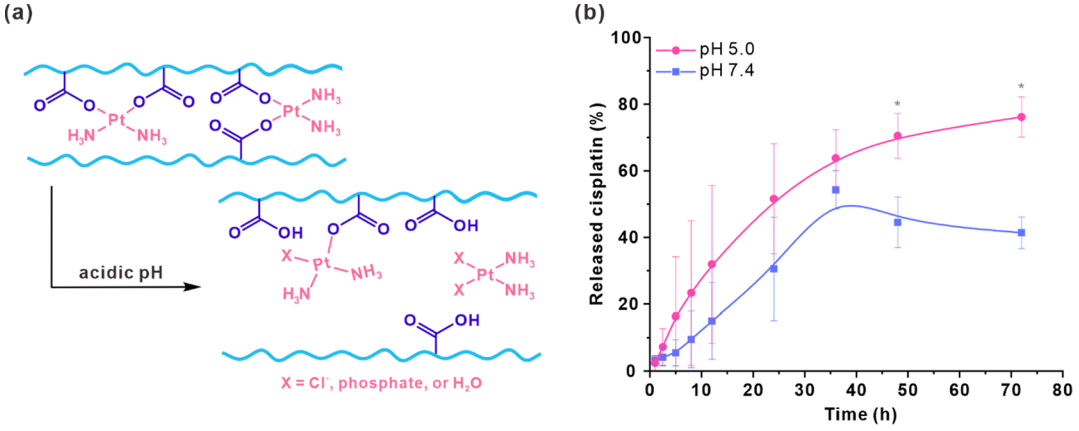

Figure 5. (a) Schematic representation of cisplatin release from the micelles under acidic pH conditions. (b) Cumulative release profiles of cisplatin from CM25 at pH 5.0 (pink circles) and 7.4 (blue squares). The average and standard deviation are reported from three independent measurements. Statistical analysis was performed through two tail Student *t* test (*p < 0.05).

Apoptosis assays using flow cytometry were conducted using an eBioscience Annexin V Apoptosis Detection Kit according to the manufacturer's instructions (Thermo Fisher Scientific). A549 cells were seeded in six-well plates with 1 × 10^6 cells/well, and the drugs were added after the cells had adhered to the wells. Once the target treatment time had elapsed, the cells were trypsinized and rinsed

https://doi.org/10.1021/acs.biomac.3c01301
Biomacromolecules XXXX, XXX, XXX−XXX

twice with cold PBS, followed by resuspension in 1× binding buffer. The cells were then stained with Annexin V and PI at room temperature for 15 min in the dark. The cells were analyzed using a flow cytometer with BD FACS software and Flowing software.

RESULTS AND DISCUSSION

Synthesis of the DOGE Monomer and Polymerization. The monomer DOGE was synthesized through a two-step reaction (Figure 1a). The successful synthesis of DOGE was verified using a variety of NMR spectroscopic techniques, including ^{1}H, ^{13}C, correlation spectroscopy (COSY), and heteronuclear single quantum correlation (HSQC) (Figures 2a and S1−S3). For example, characteristic peaks for epoxide groups (*a* and *b*; 2.56, 2.74, and 3.15 ppm) and the dimethyl substituent from oxazoline moieties (*f*; 1.24 ppm) were clearly observed in the ^{1}H NMR spectrum. The monomer was further purified by vacuum distillation prior to polymerization.

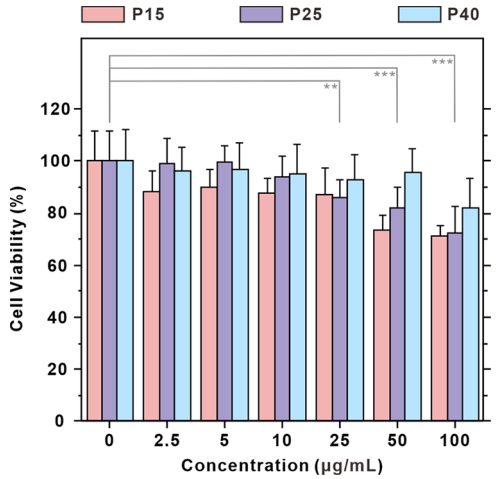

Figure 6. In vitro cell viability assay of polymers P15, P25, and P40 determined by the MTT assay using L929 cells. Statistical analysis of P25 as a model polymer was performed through two-tailed Student's *t* test (**$p < 0.01$, and ***$p < 0.001$).

After the characterization of the DOGE monomer, a series of block copolymers were synthesized via anionic ring-opening polymerization (AROP) using *m*PEG as a macroinitiator and phosphazene base *t*-BuP_4 (Figure 1b). The highly basic organic superbase *t*-BuP_4 was selected because it allows for the controlled polymerization of DOGE monomers under mild conditions.[30] Block copolymers with three different degrees of polymerization (DP: 15, 25, and 40) for the hydrophobic PDOGE blocks (polymer codes P15*, P25*, and P40*, respectively) were prepared to tailor the balance between the hydrophilic and hydrophobic blocks. As shown in Figures 2b and S4, successful polymerization was indicated by the disappearance of the epoxide peaks (*a* and *b*; 2.56, 2.74, and 3.15 ppm) and the corresponding peaks for the copolymers, including methyl protons from *m*PEG (*x*, 3.33 ppm), polyether backbone protons (*y*, *z*, and *a*′−*c*′; 3.52−4.79 ppm), methylene groups (*d*′ and *e*′; 4.07 and 4.18 ppm) and the methyl group from oxazoline moieties (*f*′; 1.24 ppm). The number-average molecular weight ($M_{n,NMR}$) and the DP were calculated as the ratio of the integral of the initiator protons to that of the methylene protons in the ^{1}H NMR spectra (Table 1 and Figure S5). Diffusion-ordered spectroscopy (DOSY) spectra also confirmed successful polymerization with a single diffusion coefficient for the respective copolymers (Figure S6). It is of note that the diffusion coefficient decreased with an increasing DP for the PDOGE blocks (7.82×10^{-7} for P15*, 5.45×10^{-7} for P25*, and 5.31×10^{-7} for P40*). In addition, the GPC results revealed that the $M_{n,GPC}$ values were close to $M_{n,NMR}$, with a monomodal distribution and narrow dispersity ($Đ$ = 1.08−1.09) for all of the copolymers (Table 1 and Figure S7).

The conversion of *m*PEG-*b*-PDOGE to *m*PEG-*b*-PGA was achieved through acidic hydrolysis, resulting in the liberation of the carboxylic acid group (Figure 1b). The ^{1}H NMR spectra revealed the disappearance of oxazoline protons at 1.24 and 4.07 ppm, confirming the successful conversion of the functional moieties (Figure 2c). Interestingly, inter- and intramolecular hydrogen bonding within the polymer chains via the polyether backbone and the carboxylic acid pendants led to the splitting of the methylene peak (*d*″, 4.16−4.22 ppm) (Figure S8). While an initial attempt to measure the $M_{n,GPC}$ of *m*PEG-*b*-PGA in water-based GPC did not produce a reliable result, an earlier report verified the conversion of PGA homopolymers via esterified PGA homopolymers.[30] Furthermore, the conversion of the oxazoline moieties to carboxylic acid groups was verified using FT-IR spectroscopy, with the imine peak at 1664 cm^{-1} observed for *m*PEG-*b*-PDOGE replaced by the carbonyl peak at 1751 cm^{-1} following conversion to *m*PEG-*b*-PGA (Figure S9).

Coordination of Cisplatin with Carboxylate in the Polymer. After the successful characterization of the polymer samples, *m*PEG-*b*-PGA was employed in a self-assembly process with cisplatin. Prior to coordination with the polymer, cisplatin was first aquated with silver nitrate ($AgNO_3$) to increase its reactivity in the ligand exchange process. The exchange of chloride ligands with water molecules was clearly verified using FT-IR spectroscopy (Figure S10). Subsequently, aquated cisplatin (*cis*-$[Pt(NH_3)_2(OH_2)_2]^{2+}$) was introduced to form coordinative linkages with the carboxylate groups in the polymer, leading to the self-assembly of micelles loaded with cisplatin. Here, the feeding ratio for cisplatin with respect to the equivalence of the carboxylate groups in the polymers was set to 0.75. In this process, the water molecules in the aquated cisplatin can readily participate in metal−ligand interactions with the carboxylate moieties, inducing the self-assembly of water-soluble DHBC polymers. These complexed micelles were labeled CM15, CM25, and CM40 in accordance with the DP of the hydrophilic blocks used (see Table S1).

The presence of coordinative interactions between the cisplatin and carboxylate groups was confirmed by using FT-IR spectroscopy. Initially, deprotected $mPEG_{114}$-*b*-PGA_{25} (i.e., P25) displayed the C═O stretching vibrations of the carboxylic acid group at 1734 cm^{-1} at pH 3 (Figure 3a). When the pH increased to 11 following the addition of 1.0 M NaOH, the asymmetric and symmetric stretching vibrations of the carboxylate groups appeared at 1599 and 1419 cm^{-1}, respectively (Figure 3b). The model micelle CM25 exhibited a C═O stretching vibration peak at 1749 cm^{-1} and asymmetric and symmetric COO^- stretching vibrations at 1595 and 1430 cm^{-1}, respectively.

Based on previous reports,[32−34] the position and separation of the asymmetric and symmetric carboxylate stretching frequencies ($\Delta\nu = \nu_{asym} - \nu_{sym.}$) are known to indicate the metal−carboxylate coordination mode (e.g., ionic, unidentate,

https://doi.org/10.1021/acs.biomac.3c01301
Biomacromolecules XXXX, XXX, XXX−XXX

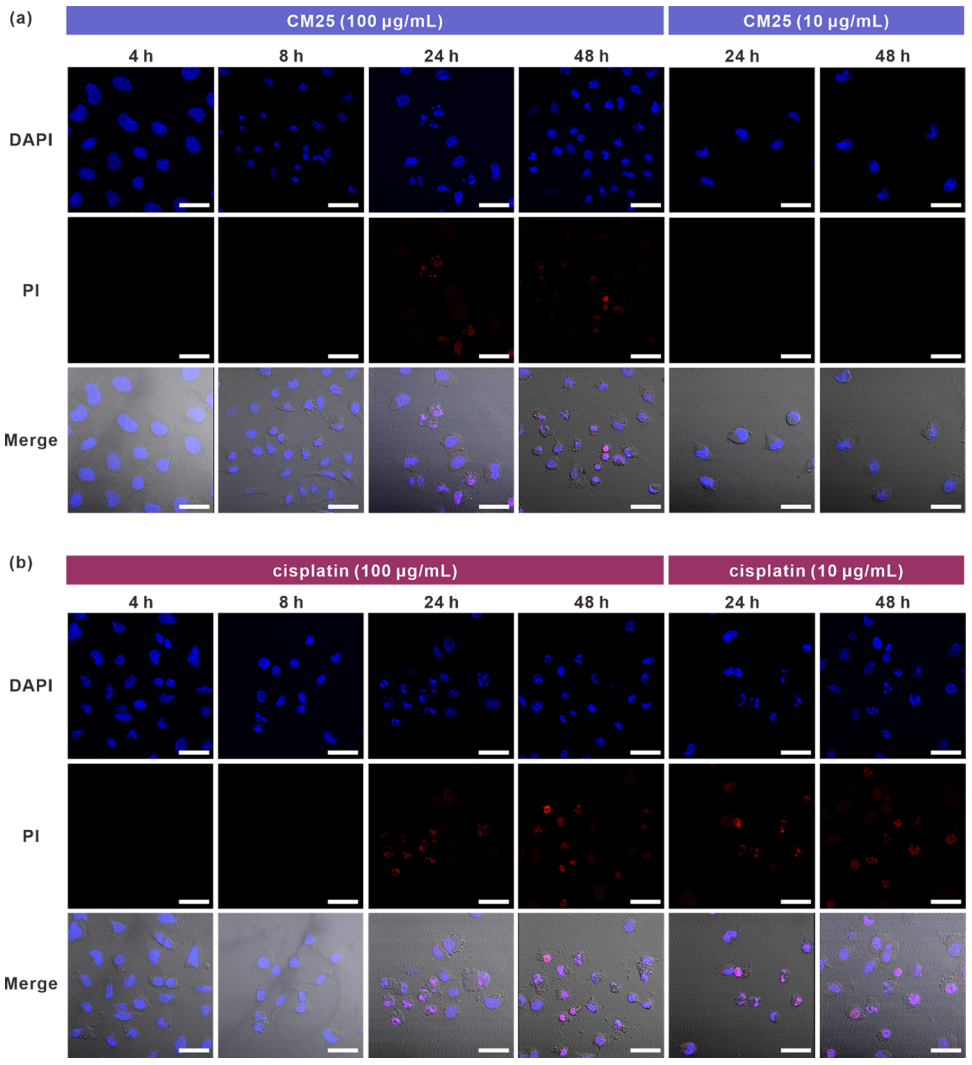

Figure 7. Confocal fluorescence microscopy images of A549 cells treated with different concentrations of (a) CM25 and (b) free cisplatin using DAPI/PI staining. The cells were incubated for a designated period of time. Scale bar: 20 μm. DAPI: 4′,6-diamidine-2′-phenylindole dihydrochloride; PI: propidium iodide.

bidentate, and bridging). The ionic mode is usually observed in the coordination of alkali metals and carboxylates.[32] The magnitude of the peak separation ($\Delta\nu$) can then be used to distinguish the unidentate ($\Delta\nu$ > 200 cm^{-1}), bidentate ($\Delta\nu$ < 110 cm^{-1}), and bridging (110 cm^{-1} < $\Delta\nu$ < 200 cm^{-1}) modes.[33,34] The peak separation observed for CM25 was 165 cm^{-1}, which corresponded to the bridging mode (Figure 3c). It should also be noted that the lower symmetrical vibration frequency of CM25 compared to P25 at pH 11 along with the strong carbonyl stretching at 1749 cm^{-1} suggested the presence of a unidentate mode in cisplatin coordination.

Independent of this observation, chemical shift changes were observed in the ^{1}H NMR spectra due to variation in electronegativity among atoms adjacent to methylene protons (Figure S11). The electronegativity of Na, H, and Pt is 0.93, 2.20, and 2.28, respectively.[35] Considering the electronegativity of the atoms connected to the carboxylate moieties, the protons neighboring the α-carbon experience deshielding, resulting in a downfield peak shift following metal−ligand exchange from the less electronegative Na to the more electronegative Pt. Taken together, these results verify the successful formation of coordination bonds between cisplatin and the polymers.

Characterization of the Micelles. The size and morphology of the micelles were characterized by using DLS and AFM (Figure 4). The feeding ratio for cisplatin with respect to the equivalence of the carboxylate groups in the polymers was varied from 0.1 to 1.0 to optimize micelle formation. DLS analysis revealed that the micelles had a monodisperse population for all of the tested feeding ratios (Figure S12). In contrast, the Pt content as determined using ICP-MS increased with a higher feeding ratio, reaching near saturation (63.3 mg/L) at a ratio of 0.75 (Figure S13). The feeding ratio was thus set to 0.75 for further analysis.

The average hydrodynamic diameter (D_h) of the micelles measured by using DLS was 186 ± 4.6 nm for CM15, 99.9 ± 1.7 nm for CM25, and 103 ± 0.9 nm for CM40 (Figure 4a−c). Interestingly, CM15, which had coordinating blocks with a low DP, formed the largest micelles. The AFM data revealed spherical micelles with an average diameter of 58.3 ± 15.5 nm for CM15, 63.9 ± 7.0 nm for CM25, and 80.9 ± 11.9 nm for CM40 that averaged over 30 micelles (Figure

https://doi.org/10.1021/acs.biomac.3c01301
Biomacromolecules XXXX, XXX, XXX−XXX

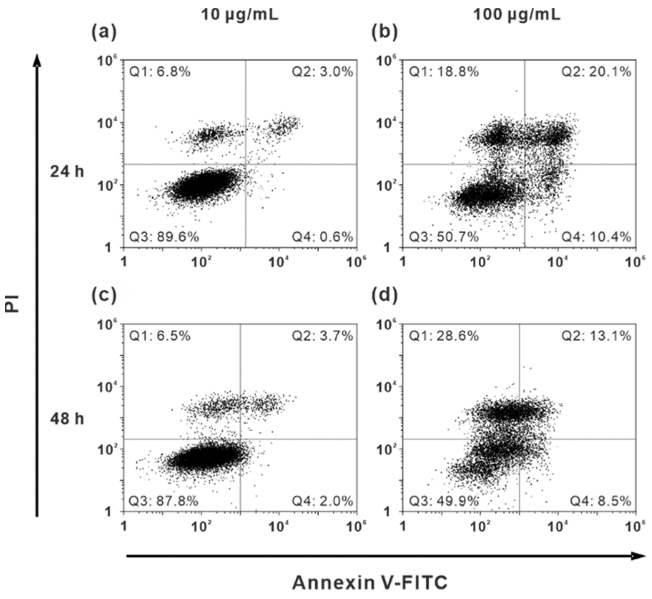

Figure 8. Flow cytometry analysis of A549 cells treated with different concentrations of CM25 using Annexin V/PI staining: (a, c) 10 and (b, d) 100 μg/mL. Each of the quadrants indicates a different category of cell death: Q1 represents necrosis, Q2 late apoptosis, Q3 live cells, and Q4 early apoptosis.

4d–f). Further experiments were conducted using CM25 as a representative sample owing to its low size distributions.

According to the ICP-MS measurements, the concentration of Pt in the micelles was determined to be 63.3 ± 1.9, 56.8 ± 0.4, and 36.0 ± 0.4 mg/L for CM15, CM25, and CM40, respectively (Figure S13). After lyophilization, the loading capacity of the micelles was estimated to be 8.14% for CM15, 7.30% for CM25, and 4.64% for CM40. As the relative fraction of PGA compared with *m*PEG increased, metal–ligand coordination was reduced, leading to a gradual decrease in the loading capacity.

Cisplatin Release Tests. The release of cisplatin from the polymeric micelles was tested in both pH 7.4 and pH 5.0 PBS. As shown in Figure 5a, the cisplatin bound to the polymer was displaced by protons under acidic conditions, and Pt forms coordination bonds with other ions such as chloride and phosphate and with water, thus generating the active form of cisplatin.[28]

The released cisplatin was collected by sampling dialyzed CM25 in PBS at 37 °C at regular time intervals. The concentration of cisplatin was determined using *o*-phenylenediamine colorimetry analysis, which generated unique absorbance at 705 nm following complexation with cisplatin (Figure S14). As shown in Figure 5b, CM25 released 51% of cisplatin within 24 h and 76% after 3 days at pH 5.0. In contrast, the release of cisplatin at pH 7.4 was lower, with a release rate of only 41% after 3 days, indicating a pH-responsive release profile. The other complexed micelles CM15 and CM40 displayed a similar pH-responsive release of cisplatin (Figure S15). It is a well-known strategy to target tumor tissues based on their acidic extracellular pH, which is a common feature of cancer cells.[36]

Cytotoxicity Assays. To assess their potential as a drug delivery system, in vitro cell viability testing with P15, P25, and P40 was conducted by using MTT assays with L929 cells. The cells remained viable at high polymer concentrations of around 100 μg/mL (Figure 6). Furthermore, the drug delivery efficiency of CM25 was compared to free cisplatin based on their IC_{50} values (Figure S16). The CM25 micelles were exposed to human lung cancer A549 cells and incubated for 48 and 72 h, respectively. According to the MTT assays, the cell viability decreased gradually with an increase in the cisplatin concentration. For example, the IC_{50} of CM25 was 57.8 μg/mL after 48 h, which decreased to 8.96 μg/mL after 72 h (Table S2). Unlike free cisplatin, which had a very low IC_{50} of 4.26 μg/mL even after 48 h of incubation, the sustained release of cisplatin from CM25 reduced the toxicity of the drug while ensuring a controlled release.[37,38]

Apoptosis Assays. To obtain detailed insights into the effect of the proposed micelles on cellular apoptosis, confocal microscopy was employed to observe cells stained with DAPI and PI. DAPI was used to stain the nucleus of both live and dead cells, while PI was employed to stain the nucleus of dead cells only. This allowed both the interactions between the micelles and the cells to be observed and the onset of programmed cell death to be pinpointed.

As shown in Figure 7, the A549 cells treated with a high concentration of CM25 (i.e., 100 μg/mL) exhibited a greater cell volume shrinkage and nucleus fragmentation as the incubation time increased. DAPI staining revealed cell contraction after 8 h, while PI staining revealed nucleus fragmentation after 24 h, confirming the occurrence of cellular apoptosis.[35] On the other hand, the cell response was markedly different when exposed to a lower concentration of CM25 and cisplatin. Under CM25 treatment, the PI staining of CM25 did not reveal any fluorescence, suggesting the absence of cell death, even after prolonged incubation for 48 h. However, cell death became evident following treatment with free cisplatin at the same concentration after 24 h. This illustrates the unique capability of the proposed micellar carrier to enhance the therapeutic efficacy of anticancer drugs in terms of delivery and the treatment of cancer cells. This observation was in good agreement with the IC_{50} values for the samples presented in Table S2.

Flow cytometry analysis was also conducted to assess the efficacy of CM25 in triggering cellular apoptosis and to quantify the number of apoptotic cells. This analysis was conducted by using Annexin V and PI fluorescence. Annexin V is employed to detect early apoptosis because it interacts with exposed phosphatidyl serine on the lipid bilayer.[39] Conversely, membrane-impermeable PI is utilized to identify late apoptotic and necrotic cells by binding to DNA. These interactions allow for the investigation of live, apoptotic, or necrotic cells based on the fluorescence exhibited by these cells.

It was found that 90% of the A549 cells treated with a low concentration of CM25 (i.e., 10 μg/mL) were alive, even after 48 h of incubation (Figure 8a,c). In contrast, following treatment with 100 μg/mL CM25, 50% of the cells were dead after 24 h, with 20% exhibiting necrosis and 30% exhibiting apoptosis (Figure 8b). After 48 h, the populations of live cells remained similar, while the primary route to cell death changed (Figure 8d). An increase in the incubation time was expected to influence the rate of necrosis, and a longer treatment duration with cisplatin did result in a higher incidence of necrotic cells.[40] Nevertheless, the flow cytometry analysis suggests that CM25 has significant potential as an effective therapeutic agent for inducing cellular apoptosis.

https://doi.org/10.1021/acs.biomac.3c01301
Biomacromolecules XXXX, XXX, XXX–XXX

CONCLUSIONS

In summary, we developed DHBC micelles to deliver cisplatin in a pH-responsive manner with low toxicity. A series of *m*PEG-*b*-PGA block copolymers were prepared via anionic ring-opening polymerization of the novel functional epoxide monomer DOGE, followed by acidic deprotection. The metal−ligand coordination between cisplatin and carboxylate in the polymer was determined to be the main driving force in the self-assembly of the DHBC into a micellar carrier. DLS and AFM analysis revealed the formation of spherical micelles that were approximately 100 nm in diameter. The micelles exhibited controlled-release kinetics for cisplatin in a pH-responsive manner, suggesting that they have potential as a passive targeting system for tumors. The micelles had considerably lower toxicity compared to free cisplatin, and the more effective sustained delivery of cisplatin was shown to induce cellular apoptosis, as evidenced by confocal fluorescence microscopy and flow cytometry. This study thus highlights the potential use of DBHCs for biomedical applications.

ASSOCIATED CONTENT

Supporting Information

The Supporting Information is available free of charge at https://pubs.acs.org/doi/10.1021/acs.biomac.3c01301.

NMR, GPC, FT-IR, DLS, ICP-MS, and UV−vis results; release profile; and MTT assay of polymers and micelles (PDF)

AUTHOR INFORMATION

Corresponding Author

Byeong-Su Kim − *Department of Chemistry, Yonsei University, Seoul 03722, Republic of Korea;* orcid.org/0000-0002-6419-3054; Email: bskim19@yonsei.ac.kr

Author

Jiwoo Yoon − *Department of Chemistry, Yonsei University, Seoul 03722, Republic of Korea;* orcid.org/0000-0003-0459-7652

Complete contact information is available at: https://pubs.acs.org/10.1021/acs.biomac.3c01301

Notes

The authors declare no competing financial interest.

ACKNOWLEDGMENTS

This work was supported by the National Research Foundation of Korea (NRF-2021R1A2C3004978 and NRF-2021M3H4A1A04092882).

REFERENCES

(1) Ghosh, S. Cisplatin: The First Metal Based Anticancer Drug. *Bioorg. Chem.* **2019**, *88*, No. 102925.

(2) Galanski, M. S.; Jakupec, M. A.; Keppler, B. K. Update of the Preclinical Situation of Anticancer Platinum Complexes: Novel Design Strategies and Innovative Analytical Approaches. *Curr. Med. Chem.* **2005**, *12* (18), 2075−2094.

(3) Qi, L.; Luo, Q.; Zhang, Y.; Jia, F.; Zhao, Y.; Wang, F. Advances in Toxicological Research of the Anticancer Drug Cisplatin. *Chem. Res. Toxicol.* **2019**, *32* (8), 1469−1486.

(4) Johnstone, T. C.; Suntharalingam, K.; Lippard, S. J. The Next Generation of Platinum Drugs: Targeted Pt(II) Agents, Nanoparticle Delivery, and Pt(IV) Prodrugs. *Chem. Rev.* **2016**, *116* (5), 3436−3486.

(5) Rocha, C. R. R.; Silva, M. M.; Quinet, A.; Cabral-Neto, J. B.; Menck, C. F. M. DNA Repair Pathways and Cisplatin Resistance: an Intimate Relationship. *Clinics* **2018**, *73*, No. e478s.

(6) Browning, R. J.; Reardon, P. J. T.; Parhizkar, M.; Pedley, R. B.; Edirisinghe, M.; Knowles, J. C.; Stride, E. Drug Delivery Strategies for Platinum-Based Chemotherapy. *ACS Nano* **2017**, *11* (9), 8560−8578.

(7) Mitchell, M. J.; Billingsley, M. M.; Haley, R. M.; Wechsler, M. E.; Peppas, N. A.; Langer, R. Engineering Precision Nanoparticles for Drug Delivery. *Nat. Rev. Drug Discovery* **2021**, *20* (2), 101−124.

(8) Cabral, H.; Miyata, K.; Osada, K.; Kataoka, K. Block Copolymer Micelles in Nanomedicine Applications. *Chem. Rev.* **2018**, *118* (14), 6844−6892.

(9) El Jundi, A.; Buwalda, S. J.; Bakkour, Y.; Garric, X.; Nottelet, B. Double Hydrophilic Block Copolymers Self-Assemblies in Biomedical Applications. *Adv. Colloid Interface Sci.* **2020**, *283*, No. 102213.

(10) Schmidt, B. V. K. J. Double Hydrophilic Block Copolymer Self-Assembly in Aqueous Solution. *Macromol. Chem. Phys.* **2018**, *219* (7), No. 1700494.

(11) Cölfen, H. Double-Hydrophilic Block Copolymers: Synthesis and Application as Novel Surfactants and Crystal Growth Modifiers. *Macromol. Rapid Commun.* **2001**, *22* (4), 219−252.

(12) Seo, E.; Kim, J.; Hong, Y.; Kim, Y. S.; Lee, D.; Kim, B. S. Double Hydrophilic Block Copolymer Templated Au Nanoparticles with Enhanced Catalytic Activity toward Nitroarene Reduction. *J. Phys. Chem. C* **2013**, *117* (22), 11686−11693.

(13) Seo, E.; Ko, S. J.; Min, S. H.; Kim, J. Y.; Kim, B. S. Plasmonic Transition via Interparticle Coupling of Au@Ag Core-Shell Nanostructures Sheathed in Double Hydrophilic Block Copolymer. for High-Performance Polymer Solar Cell. *Chem. Mater.* **2015**, *27* (13), 4789−4798.

(14) Seo, E.; Lee, S. H.; Lee, S.; Choi, S. H.; Hawker, C. J.; Kim, B. S. Highly Stable Au Nanoparticles with Double Hydrophilic Block Copolymer Templates: Correlation between Structure and Stability. *Polym. Chem.* **2017**, *8* (31), 4528−4537.

(15) Kuperkar, K.; Patel, D.; Atanase, L. I.; Bahadur, P. Amphiphilic Block Copolymers: Their Structures, and Self-Assembly to Polymeric Micelles and Polymersomes as Drug Delivery Vehicles. *Polymers* **2022**, *14* (21), 4702.

(16) Nabiyan, A.; Max, J. B.; Schacher, F. H. Double Hydrophilic Copolymers - Synthetic Approaches, Architectural Variety, and Current Application Fields. *Chem. Soc. Rev.* **2022**, *51* (3), 995−1044.

(17) Raisin, S.; Morille, M.; Bony, C.; Noel, D.; Devoisselle, J. M.; Belamie, E. Tripartite Polyionic Complex (PIC) Micelles as Non-Viral Vectors for Mesenchymal Stem Cell siRNA Transfection. *Biomater. Sci.* **2017**, *5* (9), 1910−1921.

(18) Ramasamy, T.; Poudel, B. K.; Ruttala, H.; Choi, J. Y.; Hieu, T. D.; Umadevi, K.; Youn, Y. S.; Choi, H. G.; Yong, C. S.; Kim, J. O. Cationic Drug-based Self-assembled Polyelectrolyte Complex Micelles: Physicochemical, Pharmacokinetic, and Anticancer Activity Analysis. *Colloid Surf. B* **2016**, *146*, 152−160.

(19) Frangville, C.; Li, Y.; Billotey, C.; Talham, D. R.; Taleb, J.; Roux, P.; Marty, J. D.; Mingotaud, C. Assembly of Double-Hydrophilic Block Copolymers Triggered by Gadolinium Ions: New Colloidal MRI Contrast Agents. *Nano Lett.* **2016**, *16* (7), 4069−4073.

(20) Bronich, T. K.; Keifer, P. A.; Shlyakhtenko, L. S.; Kabanov, A. V. Polymer Micelle with Cross-Linked Ionic Core. *J. Am. Chem. Soc.* **2005**, *127* (23), 8236−8237.

(21) Nishiyama, N.; Okazaki, S.; Cabral, H.; Miyamoto, M.; Kato, Y.; Sugiyama, Y.; Nishio, K.; Matsumura, Y.; Kataoka, K. Novel Cisplatin-Incorporated Polymeric Micelles Can Eradicate Solid Tumors in Mice. *Cancer Res.* **2003**, *63* (24), 8977−8983.

(22) Wang, Z.; Li, Y.; Zhang, T.; Li, H.; Yang, Z.; Wang, C. Effect of Micelle-Incorporated Cisplatin with Sizes Ranging From 8 to 40

nm for the Therapy of Lewis Lung Carcinoma. *Front. in Pharmacol.* **2021**, *12*, No. 632877.
(23) Shirbin, S. J.; Ladewig, K.; Fu, Q.; Klimak, M.; Zhang, X. Q.; Duan, W.; Qiao, G. G. Cisplatin-Induced Formation of Biocompatible and Biodegradable Polypeptide-Based Vesicles for Targeted Anticancer Drug Delivery. *Biomacromolecules* **2015**, *16* (8), 2463−2474.
(24) Huynh, V. T.; de Souza, P.; Stenzel, M. H. Polymeric Micelles with Pendant Dicarboxylato Chelating Ligands Prepared via a Michael Addition for *cis*-Platinum Drug Delivery. *Macromolecules* **2011**, *44* (20), 7888−7900.
(25) Huynh, V. T.; Chen, G. J.; de Souza, P.; Stenzel, M. H. Thiol-yne and Thiol-ene ″Click″ Chemistry as a Tool for a Variety of Platinum Drug Delivery Carriers, from Statistical Copolymers to Crosslinked Micelles. *Biomacromolecules* **2011**, *12* (5), 1738−1751.
(26) Shahin, M.; Safaei-Nikouei, N.; Lavasanifar, A. Polymeric Micelles for pH-Responsive Delivery of Cisplatin. *J. Drug Target* **2014**, *22* (7), 629−637.
(27) Suk, J. S.; Xu, Q.; Kim, N.; Hanes, J.; Ensign, L. M. PEGylation as a Strategy for Improving Nanoparticle-Based Drug and Gene Delivery. *Adv. Drug Delivery Rev.* **2016**, *99*, 28−51.
(28) Zhou, P.; Li, Z. Y.; Chau, Y. Synthesis, Characterization, and In Vivo Evaluation of Poly(Ethylene Oxide-co-Glycidol)-Platinate Conjugate. *Eur. J. Pharm. Sci.* **2010**, *41* (3−4), 464−472.
(29) Xia, Y.; Wang, Y.; Wang, Y.; Tu, C.; Qiu, F.; Zhu, L.; Su, Y.; Yan, D.; Zhu, B.; Zhu, X. A Tumor pH-Responsive Complex: Carboxyl-Modified Hyperbranched Polyether and *cis*-Dichlorodiammineplatinum(II). *Colloids Surf., B* **2011**, *88* (2), 674−681.
(30) Park, J.; Yu, Y.; Lee, J. W.; Kim, B. S. Anionic Ring-Opening Polymerization of a Functional Epoxide Monomer with an Oxazoline Protecting Group for the Synthesis of Polyethers with Carboxylic Acid Pendants. *Macromolecules* **2022**, *55* (13), 5448−5458.
(31) Surnar, B.; Sharma, K.; Jayakannan, M. Core-Shell Polymer Nanoparticles for Prevention of GSH Drug Detoxification and Cisplatin Delivery to Breast Cancer Cells. *Nanoscale* **2015**, *7* (42), 17964−17979.
(32) Lu, Y. Q.; Miller, J. D. Carboxyl Stretching Vibrations of Spontaneously Adsorbed and LB-Transferred Calcium Carboxylates as Determined by FTIR Internal Reflection Spectroscopy. *J. Colloid Interface Sci.* **2002**, *256* (1), 41−52.
(33) Barnakov, Y. A.; Idehenre, I. U.; Basun, S. A.; Tyson, T. A.; Evans, D. R. Uncovering the Mystery of Ferroelectricity in Zero Dimensional Nanoparticles. *Nanoscale Adv.* **2019**, *1* (2), 664−670.
(34) Bronstein, L. M.; Huang, X. L.; Retrum, J.; Schmucker, A.; Pink, M.; Stein, B. D.; Dragnea, B. Influence of Iron Oleate Complex Structure on Iron Oxide Nanoparticle Formation. *Chem. Mater.* **2007**, *19* (15), 3624−3632.
(35) Allred, A. L. Electronegativity Values from Thermochemical Data. *J. Inorg. Nucl. Chem.* **1961**, *17* (3), 215−221.
(36) Kato, Y.; Ozawa, S.; Miyamoto, C.; Maehata, Y.; Suzuki, A.; Maeda, T.; Baba, Y. Acidic Extracellular Microenvironment and Cancer. *Cancer Cell Int.* **2013**, *13* (1), 89.
(37) Ghosh, S.; Barman, R.; Bej, R.; Dey, P. Cisplatin-Conjugated Polyurethane Capsule for Dual Drug Delivery to a Cancer Cell. *ACS Appl. Mater. Interfaces* **2023**, *15* (21), 25193−25200.
(38) Chen, Y. Z.; Zhang, L.; Liu, Y. J.; Tan, S. M.; Qu, R. D.; Wu, Z. R.; Zhou, Y.; Huang, J. Preparation of PGA-PAE-Micelles for Enhanced Antitumor Efficacy of Cisplatin. *ACS Appl. Mater. Interfaces* **2018**, *10* (30), 25006−25016.
(39) Atale, N.; Gupta, S.; Yadav, U. C. S.; Rani, V. Cell-Death Assessment by Fluorescent and Nonfluorescent Cytosolic and Nuclear Staining Techniques. *J. Microsc.* **2014**, *255* (1), 7−19.
(40) Troyano, A.; Sancho, P.; Fernández, C.; de Blas, E.; Bernardi, P.; Aller, P. The Selection between Apoptosis and Necrosis Is Differentially Regulated in Hydrogen Peroxide-Treated and Glutathione-Depleted Human Promonocytic Cells. *Cell Death Differ.* **2003**, *10* (8), 889−898.

https://doi.org/10.1021/acs.biomac.3c01301
Biomacromolecules XXXX, XXX, XXX−XXX